

# Post-Discharge Modeling of Recent ElectricOIL Experiments

Andrew D. Palla,<sup>1</sup> David L. Carroll,<sup>2</sup> and Joseph T. Verdeyen<sup>3</sup>  
*CU Aerospace, Urbana, IL 61820*

Wayne C. Solomon<sup>4</sup>  
*University of Illinois at Urbana-Champaign, Urbana, IL 61820*

**In an electric discharge Oxygen-Iodine laser (ElectricOIL), laser action at 1315 nm on the  $I(^2P_{1/2}) \rightarrow I(^2P_{3/2})$  transition of atomic iodine is obtained by a near resonant energy transfer from  $O_2(a^1\Delta)$  which is produced using a low-pressure electric discharge. The discharge production of atomic oxygen, ozone, and other excited species adds higher levels of complexity to the post-discharge kinetics which are not encountered in a classic purely chemical  $O_2(a^1\Delta)$  generation system. In this paper we present post-discharge modeling results obtained using a modified version of the Blaze-II chemical laser code. The effects of proposed chemical kinetic reactions on post discharge kinetics were studied and simulations were compared with experimental data. The modified Blaze-II code was used to study gain and power as a function of reactant mass flow rates. While agreement with experimental data was improved with the addition of new kinetics, there still appear to be significant kinetic and mixing mechanisms that are absent from the present model.**

## I. Introduction

THE classic chemical oxygen-iodine laser (COIL) system<sup>1</sup> operates on the  $I(^2P_{1/2}) \rightarrow I(^2P_{3/2})$  [hereafter denoted  $I^*$  and  $I$ , respectively] electronic transition of the iodine atom at 1315 nm. The population inversion is produced by the near resonant energy transfer between the metastable excited singlet oxygen molecule,  $O_2(a^1\Delta)$  [also denoted  $O_2(a)$  hereafter], and the atomic iodine ground state. Conventionally, a two phase (gas-liquid) chemistry singlet oxygen generator (SOG) produces the  $O_2(a)$ . There are many system issues having to do with weight, safety and the ability to rapidly modulate the production of the  $O_2(a)$  which have motivated investigations into methods to produce significant amounts of  $O_2(a)$  using flowing electric discharges. Several investigations have been conducted into the possibility of a continuous flow hybrid electrically powered oxygen-iodine laser with electric discharges to produce the  $O_2(a)$ .<sup>2-7</sup> These studies have shown that flowing electric discharges through oxygen containing mixtures, typically diluted with a rare gas, can produce useful quantities of  $O_2(a)$ . Recent studies have demonstrated  $O_2(a)$  yields greater than 15% using electric discharges,<sup>4,5,7</sup> positive gain,<sup>8-10</sup> and cw laser power.<sup>11</sup> Several modeling studies<sup>2,5,6,12</sup> have also been performed for ElectricOIL and similar systems.

Since ElectricOIL development is impacted by an imperfect understanding of post-discharge physics, the Blaze-II chemical laser model<sup>13</sup> was improved to allow more extensive studies of ElectricOIL physics and laser performance. In this paper, we present the results of a study with an updated and more comprehensive reaction set than previously utilized. Simulations are compared with experimental data. Also presented is a study of laser gain and power as a function of reactant mass flow rates.

---

<sup>1</sup> Staff Engineer, CU Aerospace, 60 Hazelwood Drive, Champaign, IL 61820, Member AIAA.

<sup>2</sup> Engineering Director, CU Aerospace, 60 Hazelwood Drive, Champaign, IL 61820, Associate Fellow AIAA.

<sup>3</sup> Senior Scientist, CU Aerospace, 60 Hazelwood Drive, Champaign, IL 61820.

<sup>4</sup> Professor Emeritus, Univ. of Ill. at Urbana-Champaign, 104 S. Wright, Urbana, IL 61820, Associate Fellow AIAA.

## II. The Blaze-II Gas Laser Model

The Blaze-II code<sup>13</sup> was originally written to be as generic a gas laser model as possible. Blaze-II can treat arbitrary combinations of chemical species characterized by as many as 500 reactions and 40 species. Blaze-II, which contains one-dimensional fluid dynamic equations whose mixing terms were derived from the two-dimensional equations that describe the mixing flow field in a gas laser cavity, can be used for axisymmetric and 2-D flows. Lasing may occur on a single atomic transition or on as many as 10 vibrational bands of a diatomic species. Blaze-II is capable of performing premixed and mixing calculations. All simulations performed in this study assumed a premixed flow. The gain  $g$  of an iodine laser is given by<sup>14-16</sup>

$$g = \frac{7}{12} \left( \frac{A \lambda^2}{8 \pi} \right) \phi(\nu) \left( N_{I^*} - \frac{1}{2} N_I \right) \quad (1)$$

where  $\lambda = 1315$  nm,  $A = 5.0$  s<sup>-1</sup>,  $N_{I^*}$  and  $N_I$  are the number densities of excited atomic iodine, I\*, and ground state atomic iodine, I, and the Voigt lineshape function  $\phi(\nu)$  is given by

$$\phi(\nu) = \frac{2}{\Delta \nu_D} \left( \frac{\ell n 2}{\pi} \right)^{1/2} [1 - \text{erf}(y)] \exp(y^2) \quad (2)$$

where

$$\Delta \nu_D = \frac{2}{\lambda} \sqrt{\frac{2RT \ell n 2}{W}} = 1.4492 \times 10^7 \sqrt{T} \quad (3)$$

$$y = \frac{\Delta \nu_L}{\Delta \nu_D} \sqrt{\ell n 2} \quad (4)$$

$$\Delta \nu_L = P \sqrt{\frac{T_{ref}}{T}} \sum_i \alpha_i x_i \quad (5)$$

$R$  is the universal gas constant (8.314 J/mole-°K),  $W$  is the molecular weight of Iodine (126.9 gm/mole),  $T$  is the temperature in °K,  $T_{ref}$  is a reference temperature taken to be 295 °K,  $P$  is the pressure in Torr,  $x_i$  is the mole fraction of species  $i$ , and the pressure broadening coefficients  $\alpha_i$  in MHz/Torr (referenced to 295°K) are 4.4, 10.5, 7.3, 6.2, 20.6, 3.6, 3.6, and 4.7 for I, I<sub>2</sub>, O<sub>2</sub>, Cl<sub>2</sub>, H<sub>2</sub>O, He, N<sub>2</sub>, and Ar, respectively.<sup>15</sup>

The Blaze-II code was originally written to model a gas laser in which reactants are injected at a single point. The Blaze-II code was modified to permit the injection of reactants at an arbitrary number of points at arbitrary locations. This modification allows the code to better model the current ElectricOIL system in which reactants are injected at as many as four positions. Automation was added to the code that allows large parametric studies to be input, completed, and reduced quickly. The optimization of the code was substantially improved in order to further reduce run times. Blaze-II COIL runs using a 33 reaction, 12 specie set had previously required ~30 CPU seconds on an IBM RS/6000 machine,<sup>17</sup> whereas current Blaze-II ElectricOIL runs using a 98 reaction, 27 specie set now requires ~2 CPU seconds on an Intel Pentium 4 machine, and only ~1 CPU second on an Macintosh G5. Code was added to automatically reduce calculation results from multiple cases in large studies. The improvements in optimization and automation have made it possible to complete and quickly analyze large parametric studies on the order of tens of thousands of cases.

The Blaze-II cases presented in this paper are based on a four section/injection-point ElectricOIL format,<sup>9</sup> the discharge output flow, NO<sub>2</sub> injection, I<sub>2</sub> injection, and tertiary diluent (Ar/N<sub>2</sub>) injection, as shown in Fig. 1. The flow tube is approximately 4.9 cm in diameter and exhausts through a Mach 2 nozzle. Simulations begin at the exit of the discharge, which is treated as the first reactant injection point,  $X = 0$  cm. NO<sub>2</sub> is

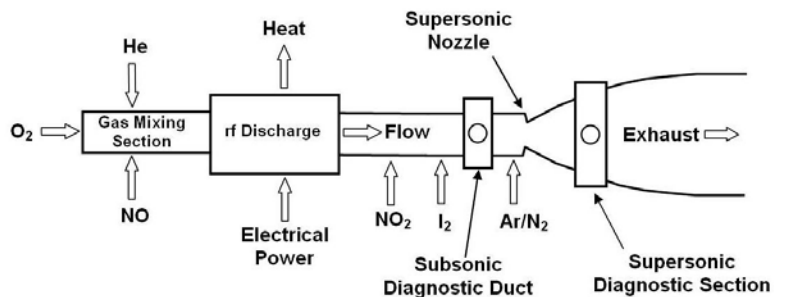


Figure 1. Schematic of ElectricOIL apparatus.

injected at  $X = 53$  cm, an  $I_2/He$  mixture is injected at  $X = 81.9$  cm, Ar or  $N_2$  is injected at  $X = 117.5$  cm, and the nozzle throat is at  $X = 141.63$  cm. The subsonic diagnostic port, hereafter referred to as the diagnostic port, is at  $X = 101.9$  cm.

### III. Blaze-II Kinetics Simulations

The accuracy of Blaze-II calculations is critically dependent on the accuracy of the input chemical kinetic reaction set. Several  $I^*$ ,  $O_2(a^1\Delta)$ , and  $O_2(b^1\Sigma)$  [also denoted  $O_2(b)$  hereafter] reactions that were not included in previous Blaze-II ElectricOIL modeling<sup>2</sup> may have affected the accuracy of the model. The following reactions were added to the model:



Reactions A, B, and D have been examined by Heaven,<sup>18</sup> Han et al,<sup>19</sup> and Vasiljeva et al,<sup>20</sup> respectively. Quenching of  $O_2(^1\Sigma)$  by various chemical species, such as  $NO_2$  in Reaction C, has been summarized by Atkinson et al.<sup>21</sup> Experiments<sup>9</sup> demonstrated the importance of controlling atomic oxygen by titrating with  $NO_2$ . Further, energetically the  $O + NO_2$  reaction is highly exothermic (2.16 eV) and therefore it is possible that significant fractions of  $O_2(a)$  and/or  $O_2(b)$  could be produced. As such, Reaction E, that includes possible branching to  $O_2(a)$  and  $O_2(b)$  was included in the model. The complete 98 reaction set, including Reactions A – D labeled Reactions 95 – 98 respectively and Reaction E branches labeled reactions 84 – 86, is listed in Table 1. Note that a number of temperature dependent reactions have been included because ElectricOIL can have as large a temperature range as 600 K at the exit of the discharge to 100 K in the supersonic laser cavity.

A baseline case used reactant molar flow rates of  $O_2:He:NO_2:I_2 = 4:16:0.2:0.008$  mmol/s and assumed a 400 Watt RF discharge producing a  $O_2(a):O_2(b):O$  yield of 12 : 0.22 : 8.0%. The yields of  $O_2(a)$ ,  $O_2(b)$ , and atomic oxygen are based upon experimental data. The fraction at the exit of the discharge ( $X = 0$ ) of  $O_2(b)$  is based upon recent experiments<sup>32</sup> that indicate the  $O_2(b)$  concentration is approximately 1.8% of the  $O_2(a)$  fraction just downstream of the discharge exit. Blaze-II cases were run with and without Reactions A and B included; the concentration of  $I^*$  as a function of axial position was plotted and found to change less than 1%. The Blaze-II case with Reactions A and B included was then compared with a case that included Reactions A – C; the concentration of  $O_2(b)$  as a function of axial position was plotted and was also found to change less than 1%. Reaction D was then added and compared to the case without Reaction D; the concentration of  $O_2(a)$  as a function of axial position was plotted and the change in  $O_2(a)$  concentration was found to decrease by approximately 5% as shown in Fig. 2. The effect of Reaction D was found to be much more significant in Refs. 7 & 20; we believe this is a consequence of their flow conditions being much slower than ours, 630 cm/s versus 2762 cm/s. While Reactions A – D do not significantly impact the results of Blaze-II ElectricOIL calculations, they have been added to the Blaze-II ElectricOIL reaction set for completeness. Reaction E is discussed in more detail below at the end of Section III.

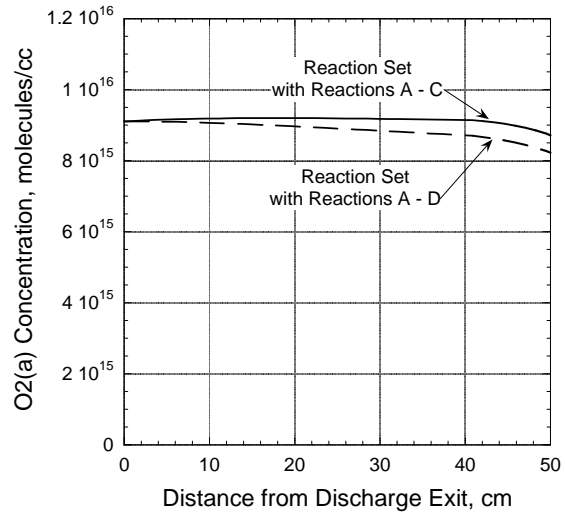


**Figure 2. Baseline ElectricOIL case with baseline reaction set including Reactions A – C and baseline reaction set including Reactions A – D. In this flow region  $[O_2(X)]$  is approximately  $8.5 \times 10^{16} \text{ cc}^{-1}$ .**

The effect of Reaction D was found to be much more significant in Refs. 7 & 20; we believe this is a consequence of their flow conditions being much slower than ours, 630 cm/s versus 2762 cm/s. While Reactions A – D do not significantly impact the results of Blaze-II ElectricOIL calculations, they have been added to the Blaze-II ElectricOIL reaction set for completeness. Reaction E is discussed in more detail below at the end of Section III.

**Table 1. Blaze-II ElectricOIL 98 reaction set and reaction rates. Reaction rates for three-body reactions have units  $\text{cm}^6/\text{molecule}^2\text{-s}$ . Certain specified quenching reactions have been assumed from other known reactions.**

$k$	Reaction						Rate, $\text{cm}^3/\text{molecule-s}$	Ref.	
1	$\text{O}_2(^1\Delta)$	+	$\text{O}_2(^1\Delta)$	$\rightarrow$	$\text{O}_2(^1\Sigma)$	+	$\text{O}_2$	$9.8e^{-28} \times T^{3.8} \times \exp(700 \times T^{-1})$	Perram <sup>23</sup>
2	$\text{O}_2(^1\Delta)$	+	$\text{O}_2(^1\Delta)$	$\rightarrow$	$\text{O}_2$	+	$\text{O}_2$	$1.7e^{-17}$	Perram <sup>23</sup>
3	$\text{O}_2$	+	$\text{O}_2(^1\Sigma)$	$\rightarrow$	$\text{O}_2(^1\Delta)$	+	$\text{O}_2$	$3.7e^{-17}$	Han <sup>24</sup>
4	$\text{O}_2(^1\Sigma)$	+	$\text{H}_2\text{O}$	$\rightarrow$	$\text{O}_2(^1\Delta)$	+	$\text{H}_2\text{O}$	$6.7e^{-12}$	Perram <sup>23</sup>
5	$\text{O}_2(^1\Sigma)$	+	$\text{Cl}_2$	$\rightarrow$	$\text{O}_2(^1\Delta)$	+	$\text{Cl}_2$	$2.0e^{-15}$	Perram <sup>23</sup>
6	$\text{O}_2(^1\Sigma)$	+	$\text{He}$	$\rightarrow$	$\text{O}_2(^1\Delta)$	+	$\text{He}$	$1.0e^{-17}$	Perram <sup>23</sup>
7	$\text{O}_2(^1\Sigma)$	+	$\text{Ar}$	$\rightarrow$	$\text{O}_2(^1\Delta)$	+	$\text{Ar}$	$1.0e^{-17}$	From #6
8	$\text{O}_2(^1\Sigma)$	+	$\text{Xe}$	$\rightarrow$	$\text{O}_2(^1\Delta)$	+	$\text{Xe}$	$1.0e^{-17}$	From #6
9	$\text{O}_2$	+	$\text{O}_2(^1\Delta)$	$\rightarrow$	$\text{O}_2$	+	$\text{O}_2$	$8.2e^{-19}$	Han <sup>24</sup>
10	$\text{O}_2(^1\Delta)$	+	$\text{H}_2\text{O}$	$\rightarrow$	$\text{O}_2$	+	$\text{H}_2\text{O}$	$4.0e^{-18}$	Perram <sup>23</sup>
11	$\text{O}_2(^1\Delta)$	+	$\text{Cl}_2$	$\rightarrow$	$\text{O}_2$	+	$\text{Cl}_2$	$6.0e^{-18}$	Perram <sup>23</sup>
12	$\text{O}_2(^1\Delta)$	+	$\text{He}$	$\rightarrow$	$\text{O}_2$	+	$\text{He}$	$8.0e^{-21}$	Perram <sup>23</sup>
13	$\text{O}_2(^1\Delta)$	+	$\text{Ar}$	$\rightarrow$	$\text{O}_2$	+	$\text{Ar}$	$8.0e^{-21}$	From #12
14	$\text{O}_2(^1\Delta)$	+	$\text{Xe}$	$\rightarrow$	$\text{O}_2$	+	$\text{Xe}$	$8.0e^{-21}$	From #12
15	$\text{O}_2(^1\Delta)$	+	$\text{N}_2$	$\rightarrow$	$\text{O}_2$	+	$\text{N}_2$	$1.4e^{-19}$	Atkinson <sup>21</sup>
16	$\text{O}_2(^1\Sigma)$	+	$\text{N}_2$	$\rightarrow$	$\text{O}_2$	+	$\text{N}_2$	$2.0e^{-16}$	Atkinson <sup>21</sup>
17	$\text{O}_2(^1\Sigma)$	+	$\text{N}_2$	$\rightarrow$	$\text{O}_2(^1\Delta)$	+	$\text{N}_2$	$1.8e^{-15}$	Atkinson <sup>21</sup>
18	$\text{O}_2(^1\Sigma)$	+	$\text{I}_2$	$\rightarrow$	$\text{O}_2$	+	$2\text{I}$	$2.8e^{-11}$	Heaven <sup>33</sup>
19	$\text{O}_2(^1\Sigma)$	+	$\text{I}_2$	$\rightarrow$	$\text{O}_2(^1\Delta)$	+	$\text{I}_2$	$2.3e^{-11}$	Han <sup>24</sup>
20	$\text{O}_2(^1\Sigma)$	+	$\text{I}_2$	$\rightarrow$	$\text{O}_2$	+	$\text{I}_2$	$6.0e^{-12}$	Heaven <sup>33</sup>
21	$\text{O}_2(^1\Delta)$	+	$\text{I}_2$	$\rightarrow$	$\text{O}_2$	+	$\text{I}_2^*$	$7.0e^{-15}$	Perram <sup>23</sup>
22	$\text{O}_2(^1\Delta)$	+	$\text{I}_2$	$\rightarrow$	$\text{O}_2$	+	$\text{I}_2$	$5.0e^{-16}$	Han <sup>24</sup>
23	$\text{I}^*$	+	$\text{I}_2$	$\rightarrow$	$\text{I}$	+	$\text{I}_2^*$	$1.4e^{-13} \times \exp(1600 \times T^{-1})$	Perram <sup>23</sup>
24	$\text{O}_2(^1\Delta)$	+	$\text{I}_2^*$	$\rightarrow$	$\text{O}_2$	+	$2\text{I}$	$3.0e^{-10}$	Perram <sup>23</sup>
25	$\text{I}_2^*$	+	$\text{O}_2$	$\rightarrow$	$\text{I}_2$	+	$\text{O}_2$	$4.9e^{-12}$	Heaven <sup>25</sup>
26	$\text{I}_2^*$	+	$\text{H}_2\text{O}$	$\rightarrow$	$\text{I}_2$	+	$\text{H}_2\text{O}$	$1.7e^{-11}$	Heaven <sup>25</sup>
27	$\text{I}_2^*$	+	$\text{He}$	$\rightarrow$	$\text{I}_2$	+	$\text{He}$	$9.8e^{-12}$	Heaven <sup>25</sup>
28	$\text{I}_2^*$	+	$\text{Ar}$	$\rightarrow$	$\text{I}_2$	+	$\text{Ar}$	$4.0e^{-12}$	Perram <sup>23</sup>
29	$\text{I}_2^*$	+	$\text{Xe}$	$\rightarrow$	$\text{I}_2$	+	$\text{Xe}$	$4.0e^{-12}$	From #28
30	$\text{I}_2^*$	+	$\text{Cl}_2$	$\rightarrow$	$\text{I}_2$	+	$\text{Cl}_2$	$6.3e^{-12}$	Heaven <sup>25</sup>
31	$\text{I}_2^*$	+	$\text{N}_2$	$\rightarrow$	$\text{I}_2$	+	$\text{N}_2$	$8.2e^{-12}$	Heaven <sup>26</sup>
32	$\text{I}^*$	+	$\text{O}_2(^1\Delta)$	$\rightarrow$	$\text{I}^*$	+	$\text{O}_2$	$2.3e^{-8} \times T^{-1}$	Perram <sup>23</sup>
33	$\text{I}^*$	+	$\text{O}_2$	$\rightarrow$	$\text{I}$	+	$\text{O}_2(^1\Delta)$	$3.1e^{-8} \times T^{-1} \times \exp(-403 \times T^{-1})$	Perram <sup>23</sup>
34	$\text{I}^*$	+	$\text{O}_2(^1\Delta)$	$\rightarrow$	$\text{I}$	+	$\text{O}_2$	$1.0e^{-15}$	Perram <sup>23</sup>
35	$\text{I}^*$	+	$\text{O}_2$	$\rightarrow$	$\text{I}$	+	$\text{O}_2$	$3.5e^{-16}$	Perram <sup>23</sup>
36	$\text{I}^*$	+	$\text{O}_2(^1\Delta)$	$\rightarrow$	$\text{I}$	+	$\text{O}_2(^1\Sigma)$	$4.0e^{-24} \times T^{3.8} \times \exp(700 \times T^{-1})$	Perram <sup>23</sup>
37	$\text{I}^*$	+	$\text{O}_2(^1\Delta)$	$\rightarrow$	$\text{I}$	+	$\text{O}_2(^1\Delta)$	$1.1e^{-13}$	Perram <sup>23</sup>
38	$\text{I}^*$	+	$\text{I}$	$\rightarrow$	$\text{I}$	+	$\text{I}$	$1.7e^{-13}$	Perram <sup>23</sup>
39	$\text{I}^*$	+	$\text{H}_2\text{O}$	$\rightarrow$	$\text{I}$	+	$\text{H}_2\text{O}$	$2.1e^{-12}$	Perram <sup>23</sup>
40	$\text{I}^*$	+	$\text{He}$	$\rightarrow$	$\text{I}$	+	$\text{He}$	$5.0e^{-18}$	Perram <sup>23</sup>
41	$\text{I}^*$	+	$\text{N}_2$	$\rightarrow$	$\text{I}$	+	$\text{N}_2$	$6.5e^{-17}$	Deakin <sup>27</sup>
42	$\text{I}^*$	+	$\text{Ar}$	$\rightarrow$	$\text{I}$	+	$\text{Ar}$	$5.0e^{-18}$	From #40
43	$\text{I}^*$	+	$\text{Xe}$	$\rightarrow$	$\text{I}$	+	$\text{Xe}$	$5.0e^{-18}$	From #40
44	$\text{I}^*$	+	$\text{Cl}_2$	$\rightarrow$	$\text{ICl}$	+	$\text{Cl}$	$5.5e^{-15}$	Perram <sup>23</sup>
45	$\text{I}^*$	+	$\text{Cl}_2$	$\rightarrow$	$\text{I}$	+	$\text{Cl}_2$	$8.0e^{-15}$	Perram <sup>23</sup>
46	$\text{I}^*$	+	$\text{ICl}$	$\rightarrow$	$\text{I}_2$	+	$\text{Cl}$	$1.5e^{-11}$	Perram <sup>23</sup>
47	$\text{I}_2$	+	$\text{Cl}$	$\rightarrow$	$\text{I}$	+	$\text{ICl}$	$2.0e^{-10}$	Perram <sup>23</sup>
48	$\text{ICl}$	+	$\text{Cl}$	$\rightarrow$	$\text{I}$	+	$\text{Cl}_2$	$8.0e^{-12}$	Perram <sup>23</sup>
49	$\text{I}_2$	+	$2\text{I}$	$\rightarrow$	$\text{I}_2$	+	$\text{I}_2$	$3.6e^{-30}$	Perram <sup>23</sup>

50	N <sub>2</sub>	+	2I	→	N <sub>2</sub>	+	I <sub>2</sub>	4.2e <sup>-33</sup>	Busch <sup>28</sup>
51	O <sub>2</sub>	+	2I	→	O <sub>2</sub> ( <sup>1</sup> Δ)	+	I <sub>2</sub>	3.7e <sup>-33</sup>	Han <sup>24</sup>
52	O <sub>2</sub>	+	2I	→	O <sub>2</sub>	+	I <sub>2</sub>	3.3e <sup>-32</sup>	Han <sup>24</sup>
53	He	+	2I	→	He	+	I <sub>2</sub>	3.8e <sup>-33</sup>	Busch <sup>28</sup>
54	I <sub>2</sub>	+	I* + I	→	I <sub>2</sub> (B)	+	I <sub>2</sub>	3.6e <sup>-30</sup>	Perram <sup>23</sup>
55			I <sub>2</sub> (B)	→	I	+	I	1.0e <sup>6</sup>	Perram <sup>23</sup>
56	2O	+	He	→	O <sub>2</sub>	+	He	4.5e <sup>-34</sup> ×exp(630×T <sup>-1</sup> )	Herron <sup>29</sup>
57	2O	+	O <sub>2</sub>	→	O <sub>2</sub>	+	O <sub>2</sub>	4.5e <sup>-34</sup> ×exp(630×T <sup>-1</sup> )	Herron <sup>29</sup>
58	2O	+	O <sub>2</sub> ( <sup>1</sup> Δ)	→	O <sub>2</sub>	+	O <sub>2</sub> ( <sup>1</sup> Δ)	4.5e <sup>-34</sup> ×exp(630×T <sup>-1</sup> )	Herron <sup>29</sup>
59	2O	+	Ar	→	O <sub>2</sub>	+	Ar	4.5e <sup>-34</sup> ×exp(630×T <sup>-1</sup> )	From #56-58
60	2O	+	Xe	→	O <sub>2</sub>	+	Xe	4.5e <sup>-34</sup> ×exp(630×T <sup>-1</sup> )	From #56-58
61	3O			→	O <sub>2</sub>	+	O	4.5e <sup>-34</sup> ×exp(630×T <sup>-1</sup> )	Herron <sup>29</sup>
62	O	+	O <sub>2</sub> + He	→	O <sub>3</sub>	+	He	5.1e <sup>-27</sup> ×T <sup>-2.8</sup>	Atkinson <sup>21</sup>
63	O	+	2O <sub>2</sub>	→	O <sub>3</sub>	+	O <sub>2</sub>	5.1e <sup>-27</sup> ×T <sup>-2.8</sup>	Atkinson <sup>21</sup>
64	O	+	O <sub>2</sub> + O <sub>2</sub> ( <sup>1</sup> Δ)	→	O <sub>3</sub>	+	O <sub>2</sub> ( <sup>1</sup> Δ)	5.1e <sup>-27</sup> ×T <sup>-2.8</sup>	Atkinson <sup>21</sup>
65	O	+	O <sub>2</sub> + Ar	→	O <sub>3</sub>	+	Ar	5.1e <sup>-27</sup> ×T <sup>-2.8</sup>	From #62
66	O	+	O <sub>2</sub> + Xe	→	O <sub>3</sub>	+	Xe	5.1e <sup>-27</sup> ×T <sup>-2.8</sup>	From #62
67	2O	+	O <sub>2</sub>	→	O <sub>3</sub>	+	O	5.1e <sup>-27</sup> ×T <sup>-2.8</sup>	Atkinson <sup>21</sup>
68	O <sub>2</sub> ( <sup>1</sup> Δ)	+	O	→	O <sub>2</sub>	+	O	2.0e <sup>-16</sup>	Herron <sup>29</sup>
69	O <sub>2</sub> ( <sup>1</sup> Σ)	+	O	→	O <sub>2</sub> ( <sup>1</sup> Δ)	+	O	7.2e <sup>-14</sup>	Atkinson <sup>21</sup>
70	O <sub>2</sub> ( <sup>1</sup> Σ)	+	O	→	O <sub>2</sub>	+	O	8.0e <sup>-15</sup>	Atkinson <sup>21</sup>
71	O <sub>2</sub> ( <sup>1</sup> Σ)	+	O <sub>3</sub>	→	2O <sub>2</sub>	+	O	1.5e <sup>-11</sup>	Atkinson <sup>21</sup>
72	O <sub>2</sub> ( <sup>1</sup> Σ)	+	O <sub>3</sub>	→	O <sub>2</sub> ( <sup>1</sup> Δ)	+	O <sub>3</sub>	3.3e <sup>-12</sup>	Atkinson <sup>21</sup>
73	O <sub>2</sub> ( <sup>1</sup> Σ)	+	O <sub>3</sub>	→	O <sub>2</sub>	+	O <sub>3</sub>	3.3e <sup>-12</sup>	Atkinson <sup>21</sup>
74	O <sub>2</sub> (ν)	+	O <sub>2</sub>	→	O <sub>2</sub>	+	O <sub>2</sub>	4.0e <sup>-14</sup>	Atkinson <sup>21</sup>
75	O <sub>2</sub> (ν)	+	He	→	O <sub>2</sub>	+	He	1.3e <sup>-13</sup>	Atkinson <sup>21</sup>
76	O	+	O <sub>3</sub>	→	O <sub>2</sub>	+	O <sub>2</sub>	8.0e <sup>-12</sup> ×exp(-2060×T <sup>-1</sup> )	Atkinson <sup>21</sup>
77	O <sub>2</sub> ( <sup>1</sup> Δ)	+	O <sub>3</sub>	→	2O <sub>2</sub>	+	O	5.2e <sup>-11</sup> ×exp(-2840×T <sup>-1</sup> )	Atkinson <sup>21</sup>
78	I <sub>2</sub>	+	O	→	IO	+	I	1.4e <sup>-10</sup>	Atkinson <sup>21</sup>
79	IO	+	O	→	O <sub>2</sub>	+	I	1.4e <sup>-10</sup>	Han <sup>24</sup>
80	IO	+	O	→	O <sub>2</sub> ( <sup>1</sup> Δ)	+	I	1.5e <sup>-11</sup>	Han <sup>24</sup>
81	IO	+	IO	→	O <sub>2</sub>	+	2I	8.2e <sup>-11</sup>	Han <sup>24</sup>
82	I	+	O <sub>3</sub>	→	IO	+	O <sub>2</sub>	2.0e <sup>-11</sup> ×exp(-890×T <sup>-1</sup> )	Atkinson <sup>21</sup>
83	I*	+	O	→	I	+	O	3.5e <sup>-12</sup>	Carroll <sup>9</sup>
84 (E)	NO <sub>2</sub>	+	O	→	O <sub>2</sub>	+	NO	6.5e <sup>-12</sup> ×exp(120×T <sup>-1</sup> )	Atkinson <sup>21</sup>
85 (E)	NO <sub>2</sub>	+	O	→	O <sub>2</sub> ( <sup>1</sup> Δ)	+	NO	0.0	Atkinson <sup>21</sup>
86 (E)	NO <sub>2</sub>	+	O	→	O <sub>2</sub> ( <sup>1</sup> Σ)	+	NO	0.0	Atkinson <sup>21</sup>
87	O	+	NO	→	NO <sub>2</sub>			2.5e <sup>-17</sup>	Kaufman <sup>30</sup>
88	O	+	NO + O <sub>2</sub>	→	NO <sub>2</sub>	+	O <sub>2</sub>	5.1e <sup>-28</sup> ×T <sup>-1.5</sup>	Atkinson <sup>21</sup>
89	O( <sup>1</sup> D)	+	O <sub>2</sub>	→	O	+	O <sub>2</sub> ( <sup>1</sup> Σ)	2.6e <sup>-11</sup> ×exp(67×T <sup>-1</sup> )	Atkinson <sup>21</sup>
90	O( <sup>1</sup> D)	+	O <sub>2</sub>	→	O	+	O <sub>2</sub> ( <sup>1</sup> Δ)	1.6e <sup>-12</sup> ×exp(67×T <sup>-1</sup> )	Atkinson <sup>21</sup>
91	O( <sup>1</sup> D)	+	O <sub>2</sub>	→	O	+	O <sub>2</sub>	4.8e <sup>-12</sup> ×exp(67×T <sup>-1</sup> )	Atkinson <sup>21</sup>
92	O( <sup>1</sup> D)	+	O <sub>3</sub>	→	2O	+	O <sub>2</sub>	1.2e <sup>-10</sup>	Atkinson <sup>21</sup>
93	O( <sup>1</sup> D)	+	O <sub>3</sub>	→	O <sub>2</sub>	+	O <sub>2</sub>	1.2e <sup>-10</sup>	Atkinson <sup>21</sup>
94	O <sub>2</sub> ( <sup>1</sup> Σ)	+	CO <sub>2</sub>	→	O <sub>2</sub> ( <sup>1</sup> Δ)	+	CO <sub>2</sub>	4.1e <sup>-13</sup>	Atkinson <sup>21</sup>
95 (A)	I*	+	NO	→	I	+	NO	1.2e <sup>-13</sup>	Heaven <sup>18</sup>
96 (B)	I*	+	NO <sub>2</sub>	→	I	+	NO <sub>2</sub>	8.5e <sup>-14</sup>	Han <sup>19</sup>
97 (C)	O <sub>2</sub> ( <sup>1</sup> Σ)	+	NO <sub>2</sub>	→	O <sub>2</sub> ( <sup>1</sup> Δ)	+	NO <sub>2</sub>	4.1e <sup>-13</sup>	Atkinson <sup>21</sup>
98 (D)	O <sub>2</sub> ( <sup>1</sup> Δ)	+	O <sub>2</sub> + O	→	2O <sub>2</sub>	+	O	1.0e <sup>-32</sup>	Vasiljeva <sup>20</sup>

Data showed that although atomic oxygen produced by the RF discharge plays a positive role in the chemistry of the laser by dissociating  $I_2$ , it also plays a negative role by quenching  $I^*$ .<sup>9</sup> In order to eliminate the negative effects of atomic oxygen,  $NO_2$  was used to scavenge some of the O atoms upstream of the  $I_2$  injection point, as shown in Fig. 1.<sup>9</sup> As such, a numerical study was performed to determine if we could model the experimental  $O_2(a)$ ,  $I^*$ , and  $O_2(b)$  concentrations, and gain data as a function of RF discharge power and  $NO_2$  flow rate with the reaction set given in Table 1. The calculations used molar flow rates of  $O_2:He:I_2 = 4:16:0.008$  mmol/s and were performed for RF discharge powers from 100 to 800 Watts (in 100 Watt increments), for each  $NO_2$  flow rate of 0.0, 0.1, 0.2, 0.5, and 1.0 mmol/s, and are presented in Figs. 3-7. The initial  $O_2(a)$  yield at the exit of the discharge was determined from ElectricOIL  $O_2(a)$  data<sup>9</sup> as a function of RF discharge power; this data had a peak  $O_2(a)$  yield of 12% at 500 Watts of RF power and flow rates of  $O_2:He = 4:16$  mmol/s at the diagnostic port position. As discussed above, the

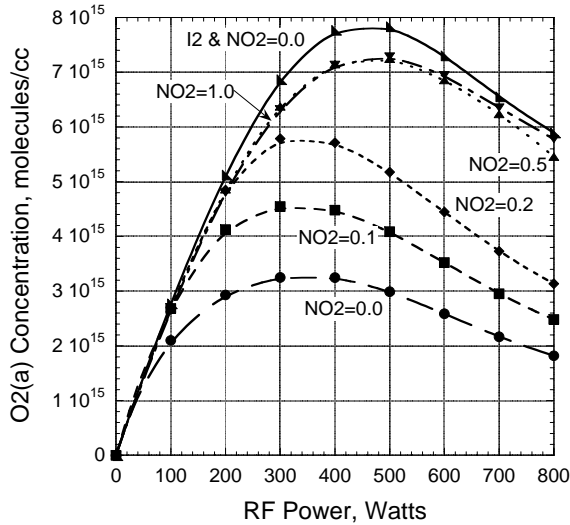


**Figure 3. Predicted  $O_2(a)$  conc. at diagnostic port vs. discharge power vs.  $NO_2$  flow rate.**

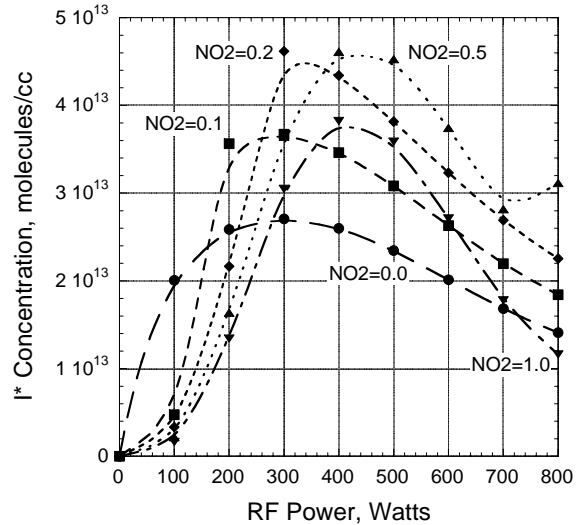


**Figure 4. Predicted  $I^*$  concentration at diagnostic port vs. discharge power vs.  $NO_2$  flow rate.**

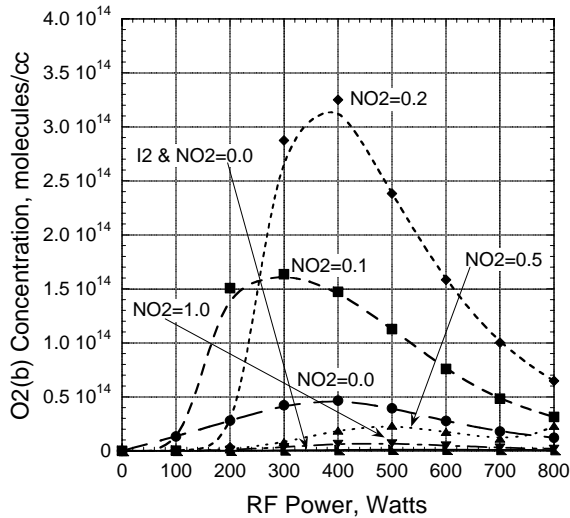


**Figure 5. Predicted  $O_2(b)$  conc. at diagnostic port vs. discharge power vs.  $NO_2$  flow rate.**

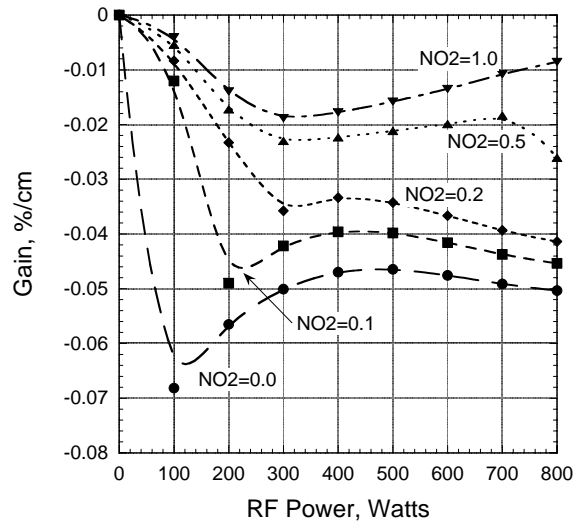


**Figure 6. Predicted gain at diagnostic port vs. discharge power vs.  $NO_2$  flow rate.**

$O_2(b)$  flow rate was approximately 1.8% of the  $O_2(a)$  flow rate.<sup>32</sup> The data from Ref. 9 showed that the production of atomic oxygen in the discharge varied linearly with discharge power such that the atomic oxygen flow rate is approximately  $7.5 \times 10^{-4}$  mmol/s per Watt of discharge power for these flow conditions. The total number of Blaze-II

simulations performed for this set of simulations was 192 (including the modeling of the individual sections for each run).

The  $\text{NO}_2$  flow rates used in ElectricOIL and Blaze-II ElectricOIL calculations are on the order of the O atom flow rate from the discharge. As a result, as discharge power and O atom production are varied as a function of discharge power for a given  $\text{NO}_2$  flow rate in the calculations, the equivalence point between the discharge production of atomic oxygen, and titration by  $\text{NO}_2$  may be crossed. Figure 7 illustrates the loss in concentration of O atoms as  $\text{NO}_2$  is added to the flow. Note that there are very few O atoms predicted at the diagnostic port position for  $\text{NO}_2$  flow rates of 0.5 and 1.0 mmol/s.

As discharge power is varied, a dramatic shift in the behavior of the model may be encountered as this equivalence point is crossed. For the cases plotted in Figs. 3 – 6 with  $\text{NO}_2$  flow rates less than or equal to 0.2 mmol/s, the discharge produced flow of O atoms is generally greater than the  $\text{NO}_2$  flow rate for all simulated discharge powers. For cases with an  $\text{NO}_2$  flow rate of 1.0 mmol/s, the discharge produced flow of O atoms is less than the  $\text{NO}_2$  flow rate for all studied discharge powers. In cases with an  $\text{NO}_2$  flow rate of 0.5 mmol/s, the discharge production of O atoms is less than the  $\text{NO}_2$  flow rate for discharge powers less than or equal to 700 Watts. The equivalence point between the discharge production of atomic oxygen and the  $\text{NO}_2$  flow rate is reached between 700 and 800 Watts of discharge power. This point is characterized by the sudden divergence of the behavior between the 0.5 mmol/s  $\text{NO}_2$  cases and the 1.0 mmol/s  $\text{NO}_2$  cases, Figs. 3 – 6.

For comparative purposes, the corresponding experimental data from Ref. [9] are illustrated here in Figs. 8-11. If we compare Figs. 3 – 6 directly with Figs. 8 – 11, respectively, it becomes clear that there are both many similarities as well as some significant differences:

1. There are strong qualitative similarities in the character of the  $\text{O}_2(\text{a})$  curves (Figs. 3 and 8) and  $\text{I}^*$  curves (Figs. 4 and 9) for  $\text{NO}_2$  flow rates of 0.0, 0.1, and 0.2. However, for  $\text{NO}_2$  flow rates of 0.5 and 1.0 there are dramatic differences.
2. There are qualitative similarities between the  $\text{O}_2(\text{b})$  (Figs. 5 and 10) and gain curves (Figs. 4 and 9) for  $\text{NO}_2$  flow rates of 0.0, 0.1, and 0.2, but again there are dramatic differences for  $\text{NO}_2$  flow rates of 0.5 and 1.0.
3. Comparing the  $\text{O}_2(\text{b})$  curves (Figs. 5 and 10) shows a significant difference for the  $\text{I}_2=0.0$  and  $\text{NO}_2=0.0$  case. In particular the predicted curve is very weak relative to the predictions for the cases with  $\text{I}_2$  and with  $\text{NO}_2$  or 0.0, 0.1, and 0.2. This suggests that there may be too much  $\text{O}_2(\text{b})$  production predicted by the model in the presence of iodine.
4. The magnitude of the predicted gain (absorption) curves is too large.

The most dramatic difference between the calculations and the data is the fact that the model does not predict the correct qualitative behavior for the high  $\text{NO}_2$  flow rates of 0.5 and 1.0 mmol/s. As noted above, these situations have an  $\text{NO}_2$  flow rate larger than the equivalence point for the quantity of atomic oxygen produced in the discharge (except for the  $\text{NO}_2=0.5$ , 800 W RF power case). The data shown in Figs. 8 – 11 suggest that significant quantities of  $\text{I}_2$  is being dissociated for the  $\text{NO}_2=0.5$  mmol/s, RF power  $\geq 300$  W cases, and for  $\text{NO}_2=1.0$  mmol/s, RF power  $\geq 400$  W cases. Because O atoms are the fastest dissociation mechanism for  $\text{I}_2$ , and because the character of the 0.5 and 1.0 mmol/s  $\text{NO}_2$  calculations do not agree with data, we theorize that the concentration of atomic oxygen is not properly represented in these premixed calculations as a result of some or all of several possible factors:

1. All of these simulations were performed as premixed calculations where all injection positions were averaged into the flow discontinuously and the calculation then proceeded downstream as fully mixed. Physically, mixing effects may cause regions of the flow where a larger percentage of atomic oxygen produced in the discharge to remain unmixed in the downstream flow than in premixed calculations.

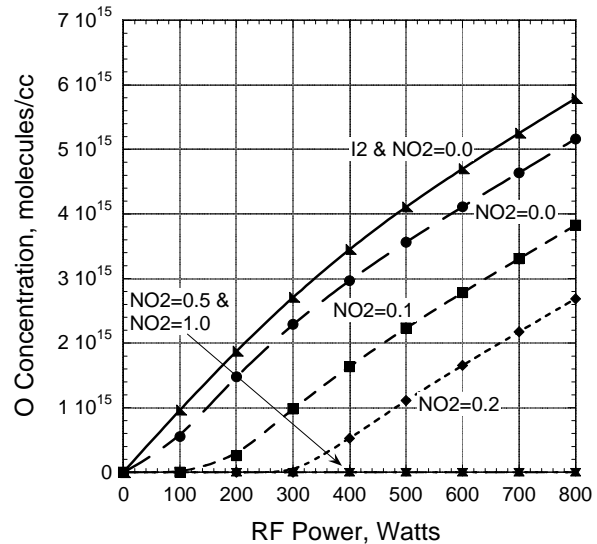


**Figure 7. Predicted O atom conc. at diagnostic port vs. discharge power vs.  $\text{NO}_2$  flow rate.**

2. Uncertainties in kinetic rates may affect the downstream concentration of atomic oxygen or other species.
3. Experimental diagnostics measuring O atom concentration do not access the entire cross-section of the flow, which may not be fully mixed. There is at least a 15-20% error associated with the experimental atomic oxygen concentration data.

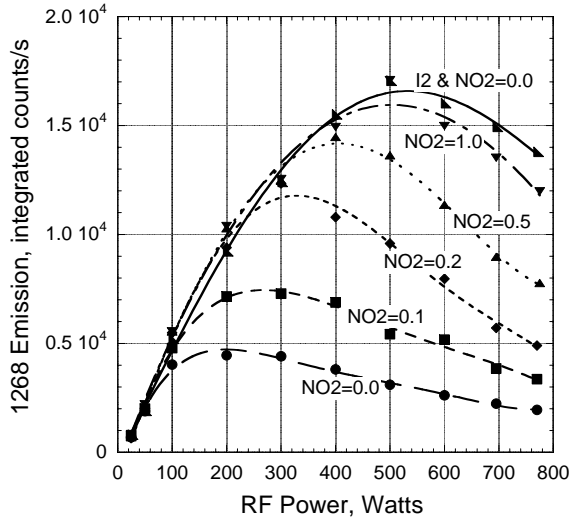


**Figure 8. Experimental O<sub>2</sub>(a) emission data from ElectricOIL at a subsonic diagnostic port vs. discharge power as a function of NO<sub>2</sub> flow rate.<sup>9</sup>**

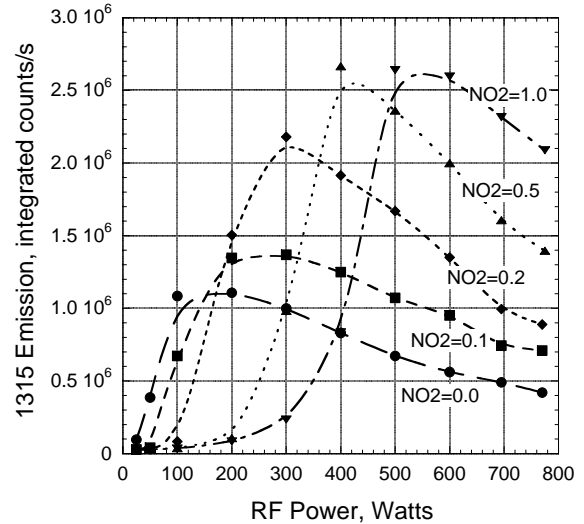


**Figure 9. Experimental I\* emission data from ElectricOIL at a subsonic diagnostic port vs. discharge power as a function of NO<sub>2</sub> flow rate.<sup>9</sup>**

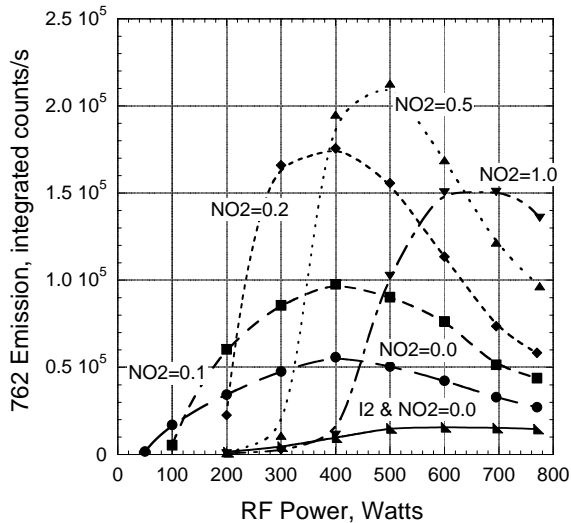


**Figure 10. Experimental O<sub>2</sub>(b) emission data from ElectricOIL at a subsonic diagnostic port vs. discharge power as a function of NO<sub>2</sub> flow rate.<sup>9</sup>**

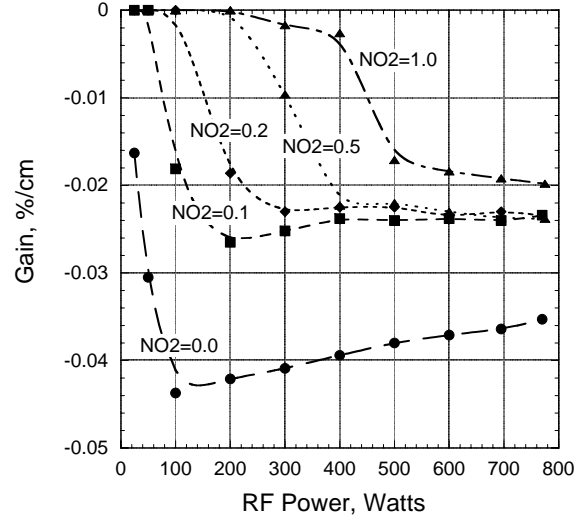


**Figure 11. Experimental gain data from ElectricOIL at a subsonic diagnostic port vs. discharge power as a function of NO<sub>2</sub> flow rate.<sup>9</sup>**

We believe that in an accurate mixing simulation, a more significant quantity of atomic oxygen produced by the discharge may remain in the flow for the requisite distance to interact with the I<sub>2</sub>, thus dissociating the I<sub>2</sub> even when there is a flow of NO<sub>2</sub> higher than the equivalence point. The mixing model is presently being updated to perform the multiple section calculations, so to test this theory using premixed calculations, the calculations were rerun with the discharge atomic oxygen yield increased by factors of 1.5, 2.0, and 3.0. Figures 12 – 16 illustrate the 300% (factor of 3.0) O atom cases; the 300% cases provided the best agreement with experimental data of the cases run. Observe that most of the qualitative trends are represented in Figs. 12 – 15 when compared with the data in Figs. 8 – 11. There are still some discrepancies between Figs. 12 – 15 and 8 – 11, but they are fewer than those shown in Figs. 3 – 6. The modeling will likely be improved by including mixing effects, better knowledge of kinetic rates, and a more accurate understanding of atomic oxygen and O<sub>2</sub>(b) yield from the electric discharge.

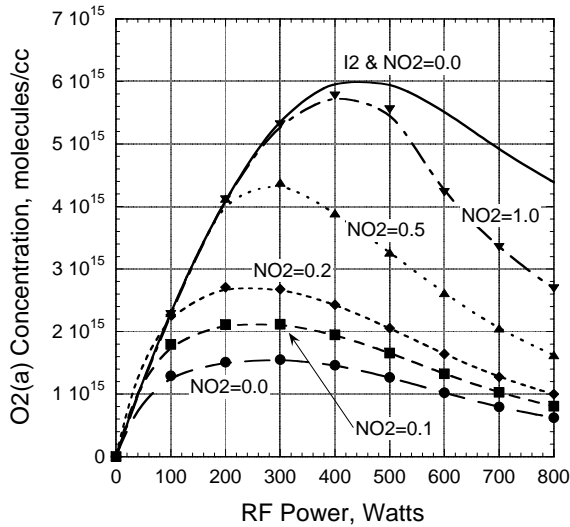


**Figure 12. Predicted  $O_2(a)$  concentration at diagnostic port vs. discharge power vs.  $NO_2$  flow rate, and 300% experimental atomic oxygen yield.**

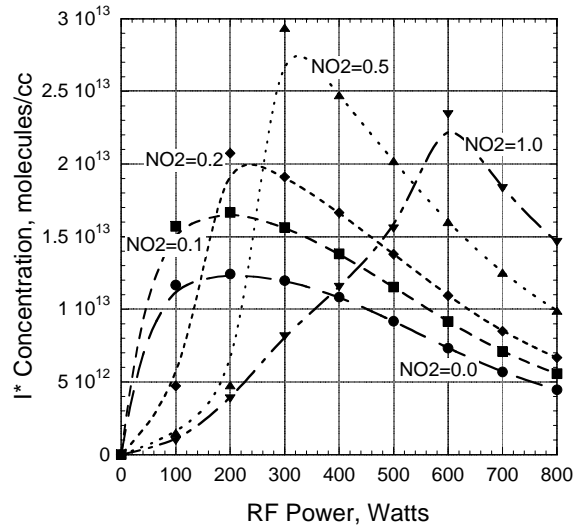


**Figure 13. Predicted  $I^*$  concentration at diagnostic port vs. discharge power vs.  $NO_2$  flow rate, and 300% experimental atomic oxygen yield.**

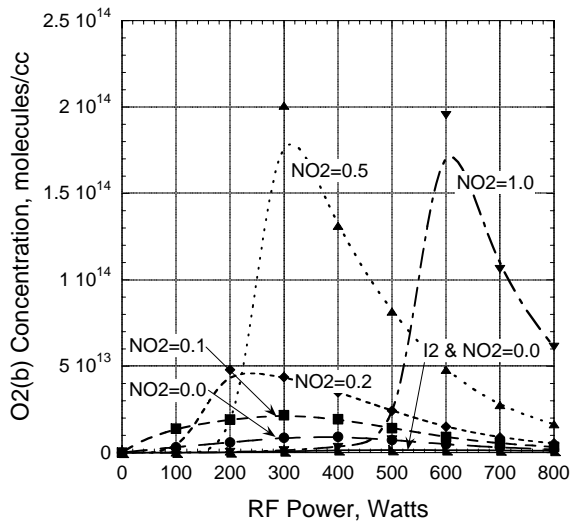


**Figure 14. Predicted  $O_2(b)$  concentration at diagnostic port vs. discharge power vs.  $NO_2$  flow rate, and 300% experimental atomic oxygen yield.**

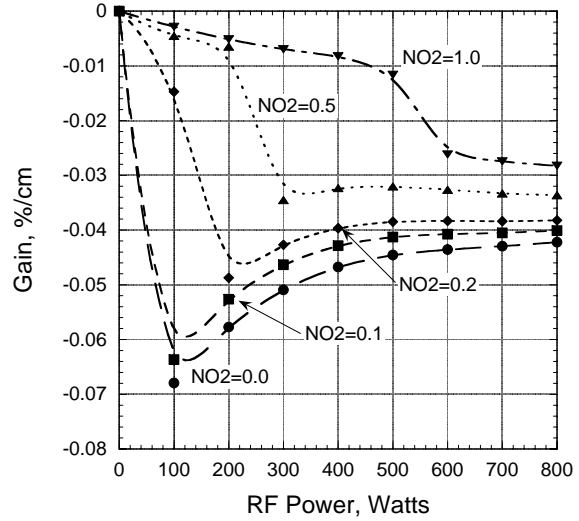


**Figure 15. Predicted gain at diagnostic port vs. discharge power vs.  $NO_2$  flow rate, and 300% experimental atomic oxygen yield.**

Figure 16 shows the loss in concentration of O atoms as  $NO_2$  is added to the flow for the 300% cases. It is seen that there are now significant quantities of O atoms predicted at the diagnostic port position for  $NO_2$  flow rates of 0.5 and 1.0 mmol/s. Note also that for RF power levels at which O atom concentrations begin to rise significantly, that these points correspond to where significant quantities of  $I_2$  are dissociated resulting in rapid (super-linear) changes in the  $I^*$  (Fig. 13),  $O_2(b)$  (Fig. 14), and the gain (Fig. 15). The more gradual changes in  $I^*$  and gain prior to having significant quantities of O atoms are believed to be the result of the slower  $O_2(b) + I_2 \rightarrow O_2 + 2I$  dissociation reaction (Table 1, reaction 18).

As discussed above, the  $NO_2 + O$  reaction is energetic enough to have branches to the  $O_2(a)$  and  $O_2(b)$  states as well as  $O_2(X)$ . The reaction  $NO_2 + O \rightarrow O_2(X^3\Sigma, v \geq 0) + NO$  has been examined by Smith et al,<sup>22</sup> and the work of others is summarized in Atkinson et al.<sup>21</sup> The total reaction rate recommended in Atkinson<sup>21</sup> is  $6.5 \times 10^{-12} \exp(120/T)$ . However, none have examined the branching fraction to  $O_2(a)$  or  $O_2(b)$ . As such, a study was undertaken to determine if this possible set of branching reactions may be playing a role by comparing calculations made with various branching ratios to data for  $O_2(a)$ ,  $I^*$ , and  $O_2(b)$  concentrations, and gain as a function of RF discharge power and  $NO_2$  flow rate. Branching ratios for Reaction E into the  $O_2 X:a:b$  states of 100:0:0, 90:10:0, 80:20:0, 70:30:0,

60:40:0, 50:50:0, 60:30:10, 50:30:20, 40:30:30, 33:33:33, 90:0:10, 75:0:25, and 50:0:50% were studied. The flow conditions were the same as used above, but were performed for RF discharge powers from 5 to 800 Watts (in 5 Watt increments). A large amount of code automation was added to make this extensive study, and the total number of Blaze-II simulations performed for this matrix of simulations was over 100,000 (including the modeling of the individual sections for each run). With the improvements made to the code for optimization, this large study was performed on two PC platforms (one Pentium 4 and one Pentium 3) running simultaneously in a total of approximately 72 CPU hours. It was found that the nominal 100% branching ratio to the  $O_2(X)$  state provided the best overall agreement with the data, while at the same time demonstrating the new ability to perform enormous kinetic studies that were previously unmanageable.

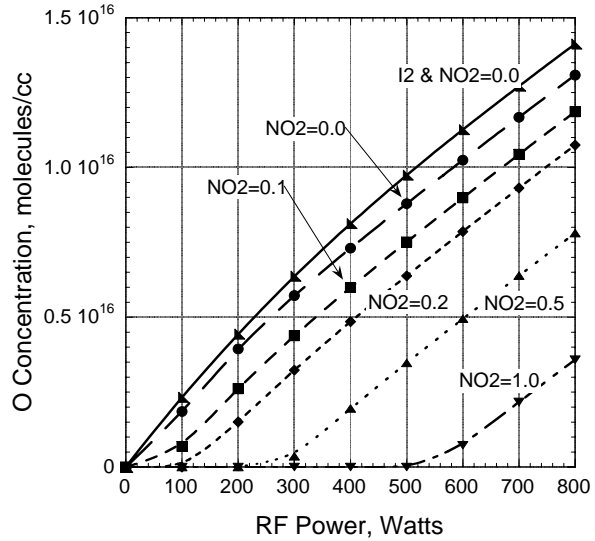


**Figure 16. Predicted O atom concentration at diagnostic port vs. discharge power vs.  $NO_2$  flow rate, and 300% experimental atomic oxygen yield.**

#### IV. Blaze-II Gain and Power Predictions

Blaze-II was used with the 98 reaction set to model current ElectricOIL gain and power data as a function of  $I_2$  flow rate and mirror reflectivities. Cases modeled used reactant flow rates of  $O_2:He:NO$  of 3:16:0.15 mmol/s with  $I_2$  flow rates of 0.008, 0.014, and 0.036 mmol/s. The 0.008 and 0.036 mmol/s  $I_2$  cases were run with two 0.99986 and two 0.99993 reflectivity mirrors respectively. The 0.014 mmol/s  $I_2$  case was run for both sets of mirror reflectivities. Simulations assumed 450 Watts of RF discharge power. The  $O_2(a)$  yield at the exit of the discharge was determined from ElectricOIL data<sup>31</sup> for  $O_2:He:NO = 3:16:0.15$  mmol/s flow conditions at 450 Watts of RF discharge power. Atomic oxygen yield was estimated to be 0.10 mmol/s at 450 Watts of RF power<sup>32</sup> from an  $NO_2$  titration experiment for the above conditions with NO in the discharge.

All of the simulations discussed in this section are premixed calculations where the injected flows are discontinuously added at the injection location and the computation is then continued as fully mixed. For the flow conditions discussed above with an RF power of 450 W, the predicted  $O_2(a)$  yield as a function of distance from the

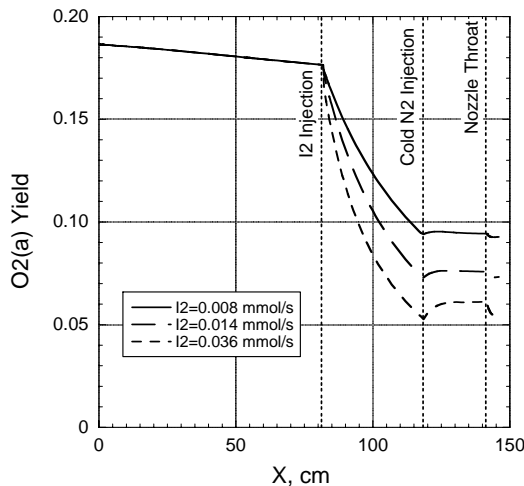


**Figure 17. Predicted  $O_2(a)$  yield vs. X and  $I_2$  flow rate for  $O_2:He:NO = 3:16:0.15$  mmol/s, 450 W RF power.**

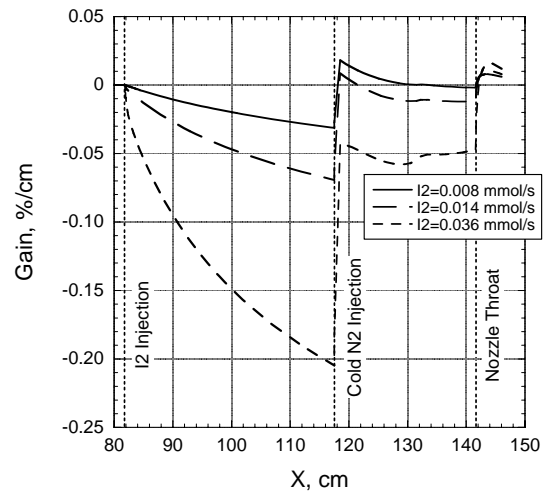


**Figure 18. Predicted gain vs. X and  $I_2$  flow rate for  $O_2:He:NO = 3:16:0.15$  mmol/s, 450 W RF power.**

discharge exit is shown in Fig. 17 for three different  $I_2$  flow rates. There are four interesting features that are observed in Fig. 17:

1. the initial drop in  $O_2(a)$  yield is principally due to the  $O_2(a)+O_2(a) \rightarrow O_2(b)+O_2$  pooling Reaction (1) and the three body quenching Reaction (98),  $O_2(a)+O_2+O \rightarrow O_2+O_2+O$ ;
2. higher  $I_2$  flow rate results in lower  $O_2(a)$  yields downstream in the laser cavity, which is in large part due to the effects of the  $I^*+O$  quenching reaction (83);
3. the rise in yield after the cold  $N_2$  injection occurs from the  $O_2(b)+N_2 \rightarrow O_2(a)+N_2$  deactivation channel, Reaction (17), where new  $O_2(b)$  has been created via  $O_2(a)+I^* \rightarrow O_2(b)+I$  after the iodine injection position;
4. the yield after the nozzle throat drops as the pumping Reaction (32) shifts in favor of  $I^*$  as the temperature drops in the supersonic expansion.

Figures 18 and 19 illustrate the predicted gain for these three  $I_2$  flow rates. A large drop in gain (increase in absorption) is observed between the  $I_2$  injection location and the  $N_2$  injection location, which is due to the  $I^*+O$  quenching that ultimately reduces both the  $I^*$  and  $O_2(a)$  concentrations. There is a sudden rise in gain when the cold  $N_2$  is injected, which is a consequence of the pumping Reaction (32) favoring colder temperatures; note that the gain then lowers as heat is transferred from the warmer wall to the cooler flow between  $N_2$  injection position and the nozzle throat (Blaze II includes a first order wall heat transfer term). Downstream of the throat the gain increases significantly in the supersonic cavity, Fig. 19. For  $I_2$  flow rates of 0.008, 0.014, and 0.036 mmol/s the peak gain in the nozzle is predicted to be approximately 0.0080 %/cm, 0.0106 %/cm, and 0.0158 %/cm, respectively. As shown in Fig. 19, the prediction of gain for both the 0.008 mmol/s of  $I_2$  and the 0.036 mmol/s of  $I_2$  cases are in reasonably good agreement with the measured gains<sup>31</sup> of 0.0067 %/cm and 0.015 %/cm, respectively, for these conditions.

Power predictions from Blaze are compared with measured data<sup>31</sup> in Fig. 20. Clearly Blaze is over-predicting the power. The Blaze calculation assumes mirrors that are the size of the flow channel, however, the experiments used 1" diameter optics with a 0.75" diameter opening that is smaller than the physical flow channel at the lasing position. As such, the Blaze calculations were adjusted lower to account for lasing in only a portion of the flow channel, however the simulation still significantly over predicts the measured power. We are presently uncertain as to why the gain is being predicted with reasonable accuracy, yet the power is not; we are investigating this issue.

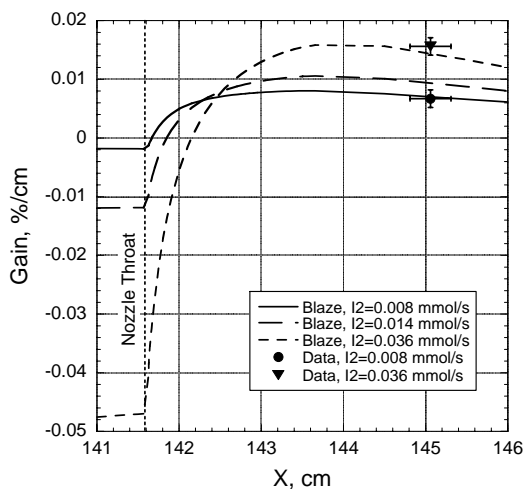


**Figure 19.** Predicted gain in the laser cavity vs.  $X$  and  $I_2$  flow rate for  $O_2:He:NO = 3:16:0.15$  mmol/s, 450 W RF power.

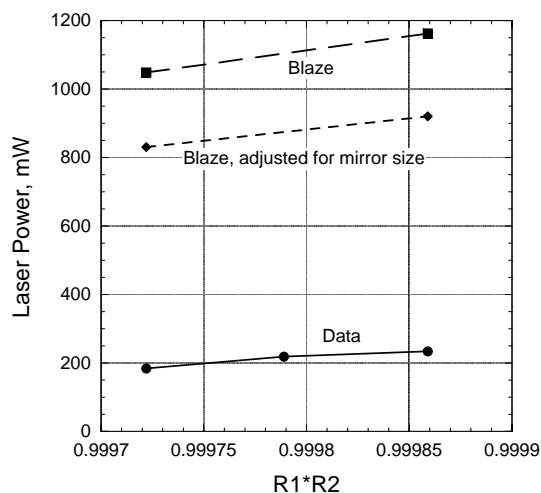


**Figure 20.** Blaze-II calculated power and ElectricOIL power vs. mirror reflectivity,  $I_2 = 0.014$  mmol/s.

## V. Concluding Remarks

Recent studies with the ElectricOIL system where the  $O_2(a^1\Delta)$  was produced in a flowing electric discharge, have demonstrated  $O_2(a^1\Delta)$  yields greater than 15%, positive gain, and cw laser power. To better understand the

post-discharge physics, premixed calculations were performed using the generic gas laser model Blaze-II. Blaze-II was adapted to allow the multiple sections/injection-points of reactants used by ElectricOIL, and was optimized to allow large parametric studies. The Blaze-II kinetic mechanism was significantly updated and now includes 98 reactions and 27 species.

Simulations were run with the updated Blaze-II model and compared with experimental data; many of the trends in the data were modeled reasonably well, but simulations with high NO<sub>2</sub> flow rates were dramatically different. We believe that these simulations did not properly represent the concentration of atomic oxygen in the flow tube principally as a result of using premixed flow calculations rather than mixing simulations. The mixing model is presently being updated to perform the multiple section calculations, so to test the hypothesis that atomic oxygen was not being properly represented the simulations were rerun with the yield of atomic oxygen increased by different factors. It was found that using 300% of experimental atomic oxygen yield allowed modeling results to provide better agreement with experimental data for I<sup>\*</sup>, O<sub>2</sub>(a<sup>1</sup>Δ), and O<sub>2</sub>(b<sup>1</sup>Σ) concentrations, and gain at the diagnostic port as a function of discharge power and NO<sub>2</sub> flow rate. We believe that a more accurate understanding of the discharge production of atomic oxygen, kinetic rates, and most importantly the use of a mixing model will improve the accuracy of future Blaze-II calculations in this respect.

Blaze-II was used with the 98-reaction set to model current ElectricOIL gain and power data as a function of I<sub>2</sub> flow rate and mirror reflectivities. Atomic oxygen yield in the simulated ElectricOIL conditions was estimated to be 0.10 mmol/s at 450 Watts of RF power using an NO<sub>2</sub> titration experiment. For the I<sub>2</sub> = 0.008 and 0.036 mmol/s cases, the gain in the supersonic cavity was modeled well by Blaze-II, however the predicted power were significantly lower. We are presently uncertain as to why the gain is being predicted with reasonable accuracy, yet the power is not; we are investigating this issue.

Overall the Blaze II model appears to be predicting many of the observed qualitative trends that have been measured, and several quantitative comparisons to data are reasonable. However, it is clear that improvements can be made with the modeling. We believe one factor that will add significantly to the accuracy of the predictions is to perform mixing simulations rather than the premixed calculations that were run in this study; the mixing model is presently being updated. Improvements in the knowledge of the kinetics will likely also play a crucial role in improved modeling of the system.

## Acknowledgements

This work was supported by the Air Force Office of Scientific Research (AFOSR) and the Missile Defense Agency (MDA) through the U.S. Army Space and Missile Defense Command (USA/SMDC). The authors would like to acknowledge the contributions of: T. Madden and G. Hager (Air Force Research Laboratory); M. Kushner (Univ. of Illinois); S. Davis, T. Rawlins and B. Kessler (PSI, Inc.); M. Heaven and K. Morokuma (Emory University); G. Perram (Air Force Institute of Technology); M. Berman (AFOSR); J. Mulroy (MDA); B. Otey (USA/SMDC); A. Ionin (P.N. Lebedev Physics Institute); A. Napartovich (Troitsk Institute for Innovation and Fusion Research); and T. Rakhimova (Lomonosov Moscow State University).

## VI. References

- <sup>1</sup>McDermott, W., Pchelkin, N., Benard, D., and Bousek, R., *Appl. Phys. Lett.* 32 (8) 469 (1978).
- <sup>2</sup>Carroll, D. L., Verdeyen, J. T., King, D. M., Woodard, B. S., Skorski, L. W., Zimmerman, J. W., and Solomon, W. C., *IEEE J. Quant. Elect.* 39 (9) 1150 (2003).
- <sup>3</sup>Carroll, D. L., Verdeyen, J. T., King, D. M., Woodard, B. S., Zimmerman, J. W., Skorski, L. W., and Solomon, W. C., "Recent Experimental Measurements of the ElectricOIL System," AIAA Paper 2003-4029 (2003).
- <sup>4</sup>Schmiedberger, J., Hirahara, S., Ichinoche, Y., Suzuki, M., Masuda, W., Kihara, Y., Yoshitani, E., and Fujii, H., *SPIE Vol.* 4184 32, (2001).
- <sup>5</sup>Hill, A. E., in *Proc. of the Int. Conf. on Lasers 2000*, ed. by V. Corcoran and T. Corcoran (STS Press, McClean, VA, 2001) 249.
- <sup>6</sup>Ionin, A. A., Klimachev, Y. M., Kotkov, A. A., Kochetov, I. V., Napartovich, A. P., Seleznev, L. V., Sinityn, D. V., and Hager, G. D., *J. Phys. D: Appl. Phys.* 36, 982 (2003).
- <sup>7</sup>Rakhimova, T. V., Kovalev, A. S., Rakhimov, A. T., Klopovsky, K. S., Lopaev, D. V., Mankelevich, Y. A., Proshina, O. V., Braginsky, O. V., and Vasilieva, A. N., "Radio-Frequency Plasma Generation of Singlet O<sub>2</sub>(a<sup>1</sup>Δ<sub>g</sub>) Oxygen in O<sub>2</sub> and O<sub>2</sub>:Ar (He) Mixtures," AIAA Paper 2003-4306 (2003).
- <sup>8</sup>Carroll, D. L., Verdeyen, J. T., King, D. M., Zimmerman, J. W., Laystrom, J. K., Woodard, B. S., Richardson, N., Kittell, K., and Solomon, W. C., *Appl. Phys. Lett.* 85 (8) 1320 (2004).
- <sup>9</sup>Carroll, D. L., Verdeyen, J. T., King, D. M., Zimmerman, J. W., Laystrom, J. K., Woodard, B. S., Benavides, G. F., Kittell, K., and Solomon, W. C., *IEEE J. Quant. Elect.* 41 (2) 213 (2005).
- <sup>10</sup>Rawlins, W.T., Lee, S., Kessler, W.J., and Davis, S.J., *Appl. Phys. Lett.* 86 051105 (2005).

- <sup>11</sup>Carroll, D. L., Verdeyen, J. T., King, D. M., Zimmerman, J. W., Laystrom, J. K., Woodard, B. S., Benavides, G. F., Kittell, K., Stafford, D. S., Kushner, M. J., and Solomon, W. C., *Appl. Phys. Lett.* **86** 111104 (2005).
- <sup>12</sup>Stafford, D. S. and Kushner, M. J., *J. of Appl. Phys.*, vol. 96., no. 5, Sept. 2004.
- <sup>13</sup>Sentman, L. H., Subbiah, M., and Zelazny, S. W., "Blaze II: A Chemical Laser Simulation Computer Program," Bell Aerospace Textron, Buffalo, NY, T.R. H-CR-77-8, February 1977.
- <sup>14</sup>Truesdell, K. A., Lamberson, S. E., and Hager, G. D., "Phillips Laboratory COIL Technology Overview," AIAA Paper 92-3003, July 1992.
- <sup>15</sup>Crowell, P. G. and Plummer, D. N., "Simplified chemical oxygen iodine laser (COIL) system model," *Intense Laser Beams and Applications*, SPIE Vol. 1871, Los Angeles, CA, pp. 148-180, 1993.
- <sup>16</sup>Crowell, P. G., "RECOIL: A One-Dimensional Chemical Oxygen Iodine Laser Performance Model: Part I - Theory," RDA Letter No. 87-A/K-3-02-1079, 15 Nov. 1989.
- <sup>17</sup>Carroll, D. L., "Modeling High-Pressure Chemical Oxygen-Iodine Lasers," AIAA Paper 94-2431, June 1994.
- <sup>18</sup>Heaven, M. C., private communication, 2004.
- <sup>19</sup>Han, J., Tinney, S. P., and Heaven, M. C., "I<sup>\*</sup> Kinetics of Relevance to Discharge Driven COIL Systems," *Proc. SPIE Vol. 5448*, pp. 261-268, Sep. 2004
- <sup>20</sup>Vasiljeva, A. N., Klopovskiy, K. S., Kovalev, A. S., Lopaev, D. V., Mankelevich, Y. A., Popov, N. A., Rakhimov, A. T., and Rakhimova, T. V., *J. Phys. D: Appl. Phys.*, **37** 2455 (2004).
- <sup>21</sup>Atkinson, R., Baulch, D. L., Cox, R. A., Hampson, R. F. Jr., Kerr, J. A., Rossi, M. J., and Troe, J., *J. of Phys and Chem. Ref. Data*, **26**, 3, pp. 550-962 (1997).
- <sup>22</sup>Smith, I. M. W., Tuckett, R. P., and Whitham, C. J., *Chem. Phys. Letter No. 0009-2614/92/*, Vol. 200, No. 6, 25 Dec. 1992.
- <sup>23</sup>Perram, G. P., and Hager, G. D., "The Standard Chemical Oxygen-Iodine Laser Kinetics Package," Air Force Weapons Laboratory, Air Force System Command, Kirtland Air Force Base, NM, Final Rep. AFWL-TR-88-50, Oct. 1988.
- <sup>24</sup>Han, J., Komissarov, A.V., Tinney, S.P., and Heaven, M. C., "Kinetic studies for advanced iodine laser concepts," *Proc. SPIE Vol. 4971*, pp. 45-56 (2003).
- <sup>25</sup>Heaven, M. C., "Studies of Energy Transfer Processes of Relevance to Chemically and Optically Pumped Lasers," Air Force Office of Scientific Research, Bolling Air Force Base, Final Rep. AFOSR-TR-95-0012, 1995.
- <sup>26</sup>Heaven, M. C., Private Communication, 1996.
- <sup>27</sup>Deakin, J. J. and Husain, D., *JCS Faraday Trans. II*, vol. 68, pp. 1603-1612, 1972.
- <sup>28</sup>Busch, G. E., *IEEE J. Quantum. Electron.*, vol. 49, no. 6, pp. 794-796, 1978.
- <sup>29</sup>Herron, J. T. and Green, D. S., *Plasma Chem. Plasma Processing*, Vol. 21, No. 3, pp. 459-481, 2001.
- <sup>30</sup>Kaufman, F., *Proc. Roy. Soc. A*, vol. 247, 1958, pp. 123-139.
- <sup>31</sup>Carroll, D. L., Verdeyen, J. T., King, D. M., Zimmerman, J. W., Laystrom, J. K., Woodard, B. S., Benavides, G. F., Richardson, N.R., Kittell, K.W., and Solomon, W. C., "Studies of CW laser oscillation on the 1315 nm transition of atomic iodine pumped by O<sub>2</sub>(a<sup>1</sup>Δ) produced in an electric discharge," submitted to *IEEE J. of Quant. Elect.* (2005).
- <sup>32</sup>Zimmerman, J.W., and King, D.M., Private Communication, 2005.
- <sup>33</sup>Heaven, M. C., private communication, 2005.